PRAMANA
— journal of
physics

Vol. 73, No. 3
September 2009
pp. 453–470

Chaotic systems in complex phase space

CARL M BENDER[1,*], JOSHUA FEINBERG[2], DANIEL W HOOK[3] and DAVID J WEIR[3]

[1]Department of Physics, Washington University, St. Louis, MO 63130, USA
[2]Department of Physics, University of Haifa at Oranim, Tivon 36006, Israel and Department of Physics, Technion, Haifa 32000, Israel
[3]Blackett Laboratory, Imperial College London, London SW7 2AZ, UK
[*]Corresponding author
E-mail: cmb@wustl.edu; joshua@technion.ac.il; d.hook@imperial.ac.uk; david.weir03@imperial.ac.uk

Abstract. This paper examines numerically the complex classical trajectories of the kicked rotor and the double pendulum. Both of these systems exhibit a transition to chaos, and this feature is studied in complex phase space. Additionally, it is shown that the short-time and long-time behaviours of these two $\mathcal{PT}$-symmetric dynamical models in complex phase space exhibit strong qualitative similarities.

Keywords. $\mathcal{PT}$ symmetry; approach to chaos; kicked rotor; standard map; double pendulum.

PACS Nos 05.45.-a; 05.45.Pq; 11.30.Er; 02.30.Hq

1. Introduction

The past decade has seen intense activity in the field of $\mathcal{PT}$ quantum mechanics [1,2]. A $\mathcal{PT}$-symmetric Hamiltonian is said to have an unbroken $\mathcal{PT}$ symmetry if its eigenfunctions are $\mathcal{PT}$ symmetric. A Hamiltonian having an unbroken $\mathcal{PT}$ symmetry is physically relevant because its eigenvalues are real and it generates unitary time evolution. Such a Hamiltonian defines a conventional quantum-mechanical theory even though it may not be Dirac Hermitian. (A linear operator is Dirac Hermitian if it remains invariant under the combined operations of matrix transposition and complex conjugation.) One can regard such non-Hermitian quantum-mechanical systems as being complex extensions of conventional quantum systems.

Interesting features of $\mathcal{PT}$ quantum mechanics have motivated many recent studies of $\mathcal{PT}$ classical mechanics. In particular, solutions to Hamilton's equations have been examined for various systems whose Hamiltonians are $\mathcal{PT}$ symmetric. For such systems the classical trajectories are typically complex [3–16]. These trajectories can lie in many-sheeted Riemann surfaces and often have elaborate topological structure. When the $\mathcal{PT}$ symmetry of the quantum Hamiltonian is not broken, the

real-energy trajectories of the corresponding classical Hamiltonian are found to be closed and periodic [8,13].

The purpose of this paper is to explore a new aspect of complex classical mechanics, namely, the complex extension of chaotic behaviour. Specifically, we study two classical systems: the kicked rotor and the double pendulum. The kicked rotor is a paradigm for studying the dynamics of chaotic systems described by time-dependent Hamiltonians [17–19]. The planar double pendulum is also a dynamical model whose classical motion is known to be chaotic [20]. The Hamiltonians for both of these dynamical systems are $\mathcal{PT}$ symmetric so long as the parameters K in the Hamiltonian for the kicked rotor (4) and g in the Hamiltonian for the double pendulum (10) are real. We use a variety of computational tools in order to derive the numerical results presented. The C programming language was used to implement a fully symplectic three-stage Gauss–Legendre Runge–Kutta method for the simulation of the double pendulum, and standard functionality in *Mathematica 6* was used in the study of the kicked rotor.

This paper is organized as follows: In §2 we define the kicked rotor and mention briefly the transition associated with the disappearance of KAM trajectories. In §3 we describe the planar double pendulum and describe the analogous transition that occurs for this dynamical system. We also reproduce the numerical work of Heyl concerning flip times. This work reveals fractal-like structure in the plane of initial conditions [21]. Then, in §§4 and 5 we study the short- and long-time behaviours of the kicked rotor and the double pendulum in the complex domain, wherein part of our objective is to identify indicators for the transition to chaos. We also demonstrate that these two very different dynamical systems exhibit remarkably similar features. Section 6 contains some concluding remarks.

2. Kicked rotor

The Hamiltonian for the kicked rotor is [17–19]

$$H = \frac{p^2}{2I} + K\cos\theta \sum_{n=-\infty}^{\infty} \delta(t - nT), \tag{1}$$

where I is the moment of inertia of the rotor, p is its angular momentum and θ is the angular coordinate. As the rotor turns, it is subjected to a periodic impulse, which is applied at times $t = 0, \pm T, \pm 2T, \ldots$. The magnitude of the impulse is proportional to K, a constant having dimensions of angular momentum. This Hamiltonian is $\mathcal{PT}$ symmetric because it is symmetric separately under the operation of angular reflection $\mathcal{P}$, where $\mathcal{P}$: $\theta \to 2\pi - \theta$ and $\mathcal{P}$: $p \to -p$, and the operation of time reversal $\mathcal{T}$, where $\mathcal{T}$: $t \to -t$, $\mathcal{T}$: $p \to -p$, and $\mathcal{T}$ leaves θ invariant. (Note that angular reflection $\mathcal{P}$ is not the same as spacial reflection, which maps $\theta \to \pi - \theta$.)

Hamilton's equations of motion derived from (1) are

$$\frac{\mathrm{d}\theta}{\mathrm{d}t} = \frac{p}{I} \quad \text{and} \quad \frac{\mathrm{d}p}{\mathrm{d}t} = K\sin\theta \sum_{n=0}^{\infty} \delta(t - nT). \tag{2}$$

These equations imply that the angular momentum p changes discontinuously at each kick, but remains constant between kicks. As a result, the angle θ changes linearly with time t between kicks and is continuous at each kick.

It is customary to denote $p_n = p(nT + 0^+)$ and $\theta_n = \theta(nT + 0^+)$. Thus, p_n is the angular momentum and θ_n is the angle variable immediately after the nth kick. These variables satisfy the discretized version of (2):

$$\theta_{n+1} = \theta_n + \frac{T}{I} p_n \quad \text{and} \quad p_{n+1} = p_n + K \sin \theta_{n+1}. \tag{3}$$

It is conventional to replace p_n and K by the dimensionless quantities $\frac{T}{I} p_n \to p_n$ and $\frac{T}{I} K \to K$, in terms of which we rewrite (3) in dimensionless form as

$$\theta_{n+1} = \theta_n + p_n \quad \text{and} \quad p_{n+1} = p_n + K \sin \theta_{n+1}. \tag{4}$$

This system of difference equations, which depends on a single dimensionless real parameter K, is known as the standard map. It is straightforward to show that the standard map is area-preserving in $p - \theta$ phase space. The angular variable θ_n may be taken modulo 2π. It then follows from the first equation in (4) that p_n may also be taken modulo 2π. Thus, (4) maps the two-dimensional torus onto itself.

The behaviour of the standard map (4) has been studied extensively [17–19,22–26]. For small K the motion in phase space is bounded and chaotic in some regions. As K increases, KAM trajectories disappear. At the critical value $K_c = 0.9716\ldots$ only the KAM trajectories with golden-mean winding number and with inverse golden-mean winding number remain, and the motion in phase space is still confined. For $K > K_c$ the last bounding trajectory is destroyed and global diffusion in phase space ensues. The critical behaviour near K_c has been studied intensively [23,26].

Figure 1 illustrates the transition from subcritical to supercritical K for the kicked rotor. In this figure we display four sets of superpositions of phase planes, each consisting of 11 randomly chosen initial conditions θ_0, p_0. For each set of initial conditions we allow the time variable n to range from 1 to several thousand. The values of K for these four plots are 0.40, 0.97, 2.0 and 4.0.

In this paper we continue the classical dynamics described by the standard map (4) into complex phase space [26a]. Our objective here is to generalize (4) into complex phase space and thereby gain a better understanding of the critical behaviour near K_c. To accomplish this we are motivated to extend the analysis of refs [3–16] to time-dependent systems. Thus, we treat p_n, θ_n and sometimes K as complex variables, which we separate into real and imaginary parts as

$$p_n = r_n + i s_n, \quad \theta_n = \alpha_n + i\beta_n, \quad K = L + iM. \tag{5}$$

Substituting (5) in (4), we obtain the complexified standard map

$$\begin{aligned}
&\alpha_{n+1} = \alpha_n + r_n, \quad \beta_{n+1} = \beta_n + s_n, \\
&r_{n+1} = r_n + L \sin \alpha_{n+1} \cosh \beta_{n+1} - M \cos \alpha_{n+1} \sinh \beta_{n+1}, \\
&s_{n+1} = s_n + L \cos \alpha_{n+1} \sinh \beta_{n+1} + M \sin \alpha_{n+1} \cosh \beta_{n+1}.
\end{aligned} \tag{6}$$

In §§4 and 5 we display and discuss the results of our numerical studies of (6).

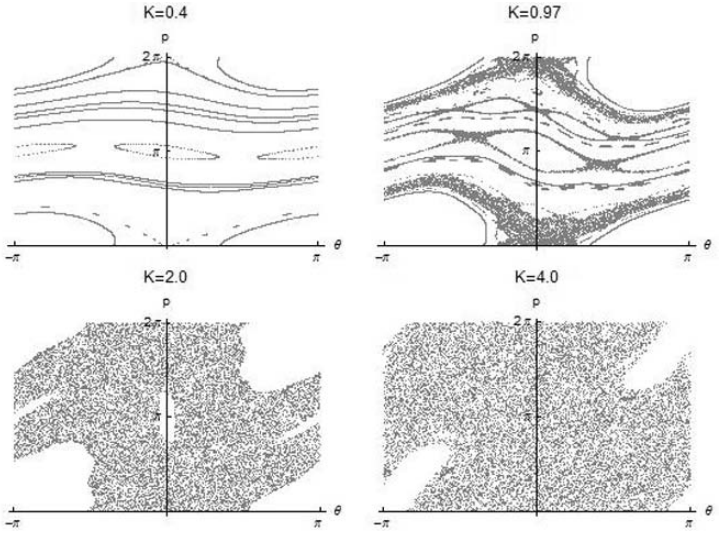

Figure 1. Four phase-plane views of the kicked rotor. In each of the figures we display the superposition of the discrete phase-plane trajectories θ_n, p_n for 11 randomly chosen initial conditions. The time variable n ranges from 1 to several thousand. The values of K for the four plots are 0.40, 0.97, 2.0 and 4.0. The KAM surfaces separate Poincaré islands. As K increases, the KAM surfaces gradually disappear and the trajectories diffuse into the phase plane.

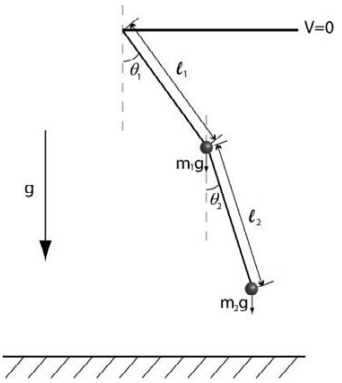

Figure 2. Configuration of the double pendulum. The double pendulum consists of two massless rods, each having a massive bob at the end. The second rod hangs from the end of the first rod. The two rods swing in a plane and are acted on by a homogeneous gravitational field of strength g.

3. Double pendulum

As shown in figure 2, a planar double pendulum consists of a massless rod of length ℓ_1 with a bob of mass m_1 at the lower end from which hangs a second massless rod

of length ℓ_2 with a second bob of mass m_2. This compound pendulum swings in a homogeneous gravitational field g, and its motion is constrained to a plane.

In this paper we take both bobs to have unit mass and both rods to have unit length. The coordinates of the bobs in terms of the angles from the vertical are

$$\begin{aligned} x_1 &= \sin\theta_1, \quad y_1 = -\cos\theta_1, \\ x_2 &= \sin\theta_1 + \sin\theta_2, \quad y_2 = -\cos\theta_1 - \cos\theta_2. \end{aligned} \tag{7}$$

Therefore, the potential and kinetic energies of the double pendulum are

$$V = -g\cos\theta_2 - 2g\cos\theta_1 \quad \text{and} \quad T = \dot{\theta}_1^2 + \tfrac{1}{2}\dot{\theta}_2^2 + \dot{\theta}_1\dot{\theta}_2\cos(\theta_1 - \theta_2). \tag{8}$$

From these one can form the Lagrangian $L = T - V$, and then construct the Hamiltonian for the system by a Legendre transform. We obtain

$$H = \frac{p_1^2 + 2p_2^2 - 2p_1p_2\cos(\theta_1 - \theta_2)}{2\left[\sin^2(\theta_1 - \theta_2) + 1\right]} - g\cos\theta_2 - 2g\cos\theta_1. \tag{9}$$

This Hamiltonian is $\mathcal{PT}$ symmetric because it is symmetric separately under angular reflection $\mathcal{P}$, where $\mathcal{P}$: $\theta_{1,2} \to 2\pi - \theta_{1,2}$ and $\mathcal{P}$: $p_{1,2} \to -p_{1,2}$, and time reversal $\mathcal{T}$, where $\mathcal{T}$: $t \to -t$, $\mathcal{T}$: $p_{1,2} \to -p_{1,2}$, and $\mathcal{T}$ leaves $\theta_{1,2}$ invariant.

Hamilton's equations are then

$$\begin{aligned} \dot{p}_1 &= -\frac{\partial H}{\partial \theta_1} = -2g\sin\theta_1 - \frac{p_1p_2\sin(\theta_1 - \theta_2)}{\sin^2(\theta_1 - \theta_2) + 1} \\ &\quad + \frac{[p_1^2 + 2p_2^2 - 2p_1p_2\cos(\theta_1 - \theta_2)]\sin[2(\theta_1 - \theta_2)]}{2[\sin^2(\theta_1 - \theta_2) + 1]^2}, \\ \dot{\theta}_1 &= \frac{\partial H}{\partial p_1} = \frac{p_1 - p_2\cos(\theta_1 - \theta_2)}{\sin^2(\theta_1 - \theta_2) + 1}, \\ \dot{p}_2 &= -\frac{\partial H}{\partial \theta_2} = -g\sin\theta_2 + \frac{p_1p_2\sin(\theta_1 - \theta_2)}{\sin^2(\theta_1 - \theta_2) + 1} \\ &\quad - \frac{[p_1^2 + 2p_2^2 - 2p_1p_2\cos(\theta_1 - \theta_2)]\sin[2(\theta_1 - \theta_2)]}{2[\sin^2(\theta_1 - \theta_2) + 1]^2}, \\ \dot{\theta}_2 &= \frac{\partial H}{\partial p_2} = \frac{2p_2 - p_1\cos(\theta_1 - \theta_2)}{\sin^2(\theta_1 - \theta_2) + 1}. \end{aligned} \tag{10}$$

Note that this system conserves energy, unlike the kicked rotor whose Hamiltonian (1) is time-dependent.

A beautiful and convincing numerical demonstration that the motion of the double pendulum is complicated and elaborate was given by Heyl [21]. In his work Heyl calculates for a given initial condition the time required for either pendulum to exhibit a flip; that is, for either θ_1 or θ_2 to exceed the value π. This calculation is then performed for the limited set of initial conditions for which $p_1(0) = 0$ and $p_2(0) = 0$, and the initial values of θ_1 and θ_2 both range from 0 to 2π. Each pixel in the initial θ_1, θ_2 plane is then coloured according to the length of the flip time.

We have applied Heyl's approach to the double pendulum in (10) and have used a Gauss–Legendre Runge–Kutta method, which is known to be fully symplectic

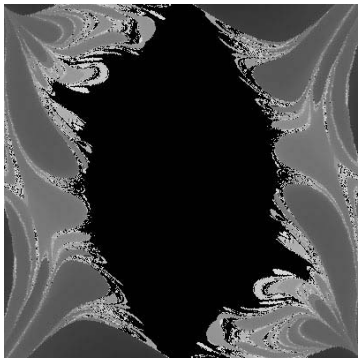

Figure 3. Flip times for initial conditions $-\pi \leq \theta_1(0) \leq \pi$, $-\pi \leq \theta_2(0) \leq \pi$, $p_1(0) = 0$ and $p_2(0) = 0$. By a flip we mean that the angular position of either bob exceeds π. This figure contains a 600×600 grid of pixels. The colour of each pixel characterizes the behaviour of the double pendulum that arises from the initial condition $[\theta_1(0), \theta_2(0)]$. If neither pendulum flips within 100 time units, then the pixel is black (the convex-lens-shaped region in the centre of the figure). If one of the pendula flips in a short time, the pixel is coloured dark gray. Longer flip times are indicated by lighter shades of gray. The fractal-like structure throughout the diagram reveals the nontrivial dynamics of the double pendulum. Because of parity symmetry this figure is symmetric under the combined reflections $\theta_{1,2} \to -\theta_{1,2}$. Note that different pixels are associated with different energies and that there is an elliptical region at the centre of the figure in which flips are forbidden by energy considerations.

[31,32]. The results of this calculation are given in figure 3. This figure is composed of a 600×600 grid of pixels, where each pixel represents the initial condition $[\theta_1(0), \theta_2(0)]$. If neither pendulum flips within 100 time units, then the pixel is assigned the colour black (the convex-lens-shaped region in the centre of the figure). If either pendulum flips in a short time, the pixel is coloured dark gray, with longer flip times being indicated by lighter shades of gray. Notice the fractal-like structure throughout the diagram. The appearance of this complicated structure demonstrates that even though the double pendulum has only two degrees of freedom, it exhibits rich and nontrivial dynamics.

In analogy with the kicked rotor, there is a transition in the behaviour of the double pendulum in which KAM surfaces disappear as a dimensionless parameter increases beyond a critical value. This parameter, which measures the strength of the gravitational field relative to the total energy, is defined as [20] $\gamma \equiv m_1 g \ell_1 / E$. The transition occurs near $\gamma = 0.1$ and ref. [20] shows that at the transition the last surviving KAM surface is the one with winding number being equal to the golden mean. In figure 4 we plot the Poincaré sections generated from 25 randomly chosen initial conditions for four different values of γ. The plot displays points in the θ_1, p_1 plane when $\theta_2 = 0$ and simultaneously $p_2 > 0$. A KAM surface is visible when $\gamma = 0.05$, which is below the critical value. At $\gamma = 0.1$, which is near the critical value, the KAM surface disappears. For the other two values of γ, which are significantly greater than the critical value, the distribution of points in the plot

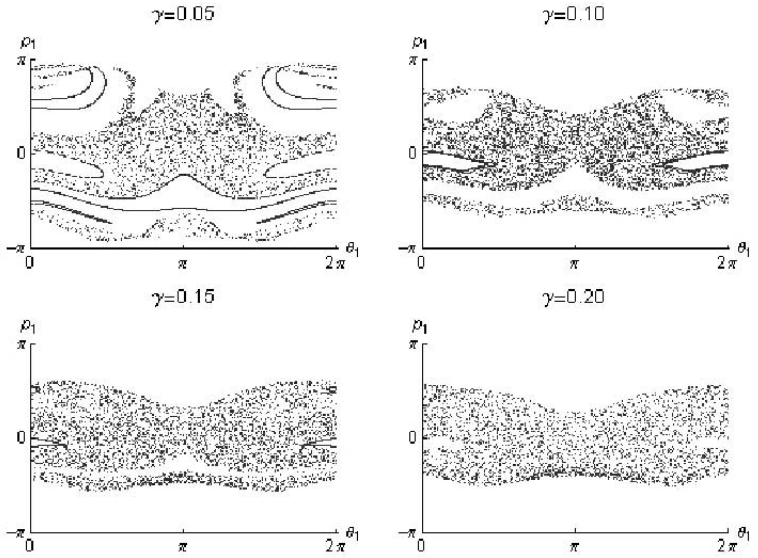

Figure 4. Poincaré plots for the double pendulum for four values of γ. Below the critical value, which is near $\gamma = 0.1$, the final KAM surface can still be seen in the second plot, but this surface evaporates as γ increases past the critical value and the points in the plot spread. This plot is analogous to that in figure 1 for the kicked rotor.

becomes diffuse in a manner analogous to the behaviour displayed in figure 1 for the kicked rotor in the $K > K_c$ regime.

4. Short-time behaviour

Having reviewed some properties of the kicked rotor and the double pendulum, we proceed to examine the behaviour of the solutions to the kicked rotor and double pendulum equations of motion in the complex domain. To do so, we do not change the form of the equations of motion, but rather we take complex initial conditions and in some cases we allow the parameter K in (4) for the kicked rotor and the parameter g in (10) for the double pendulum to take on complex values.

In this section we investigate the behaviour of these dynamical systems for short times; that is, for up to 1000 time steps. For the kicked rotor, let us see what happens if we take the initial momentum to be real, $p_0 = 0$, but take the initial angle to have a small imaginary component, $\theta_0 = 1 + 0.0001i$. In figure 5 we plot the points θ_n in the complex-θ plane for $n = 0, 1, 2, \ldots, 1000$ for a range of real values of K around the critical point $K_c = 0.9716\ldots$. While it is difficult to see the subtle change from subcritical to supercritical behaviour in real plots like those in figure 1, a qualitative change in the complex behaviour is quite evident in figure 5 [33]. Below K_c the points tend to occupy a two-dimensional region in the complex plane with some fine structure in it, but as K increases above K_c, the points tend to coalesce along well-separated one-dimensional curves.

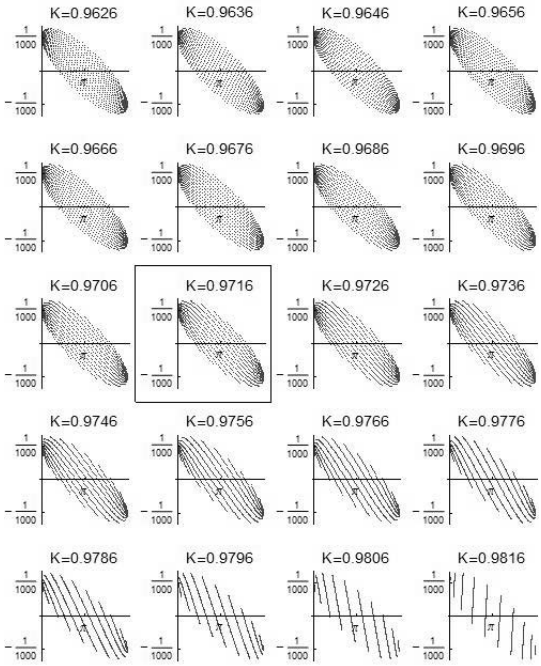

Figure 5. Behaviour of the solution to the kicked rotor in the complex-θ plane for a range of real values of K near $K_c = 0.9716\ldots$. We take as an initial condition $p_0 = 0$ and $\theta_0 = 1 + 0.0001i$ and allow the system to evolve for $n = 1000$ time steps. For each value of n we plot the complex value of θ_n as a point in the complex-θ plane. The plot corresponding to the critical value is highlighted. Note that there is a qualitative change in the nature of these complex plots as K passes through its critical value. Specifically, the points making up the plot become less uniform and more stratified. These changes in behaviour are easier to observe than those in figure 1.

In analogy with figure 5, we plot in figure 6 a trajectory for the double pendulum in the $\mathrm{Re}\,\theta_1$, $\mathrm{Im}\,p_2$ plane as a function of t for $0 \le t \le 224$. We take two values of γ, one subcritical and one supercritical, and use the slightly complex initial conditions $\theta_1 = 3.1$, $\theta_2 = 3.1 + 0.0001i$, $p_1 = 1.283$ and $p_2 = 1.283$ in which the numbers are chosen at random. When γ is above the critical value the trajectory appears to be confined to distinct narrow bands, somewhat similar to the stratified structures that occur for $K > K_c$ in figure 5 for the kicked rotor. However, when γ is below the critical value, the trajectory spreads and is similar to the more diffuse behaviour in figure 5 when $K < K_c$. It would be interesting to understand this stratification analytically and also to understand its relation to KAM theory.

A more dramatic way to observe the transition from the subcritical to the supercritical regions of the kicked rotor is to construct plots like that in figure 3 for the double pendulum. We take $p_0 = 0$ and take a range of complex initial values for θ_0: $-\pi \le \mathrm{Re}\,\theta_0 \le \pi$ and $-\pi \le \mathrm{Im}\,\theta_0 \le \pi$. For each initial condition we allow the kicked rotor to evolve up to a maximum of 400 time steps and determine the time

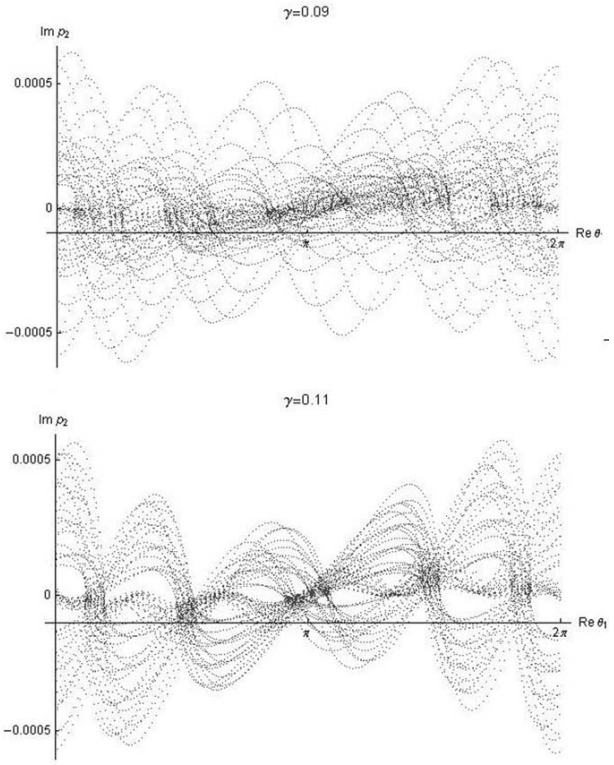

Figure 6. Trajectory for the double pendulum resulting from the slightly complex initial conditions $\theta_1 = 3$, $\theta_2 = 3 + 0.0001i$, $p_1 = p_2 = 2$. The parameter γ is varied by changing the values of g and l_1 and fixing $m_1 = E = 1$. This plot displays the trajectory in the $\mathrm{Re}\,\theta_1$, $\mathrm{Im}\,p_2$ plane as a function of t for $0 \leq t \leq 1000$. The trajectory is confined to narrow bands when γ is above the critical value and is more diffuse when it is below the critical value. In this sense, this is similar to figure 5 for the kicked rotor.

step at which the real part of p_n becomes infinite, if it does become infinite. (Here, by infinite we mean that the numerical value of $\mathrm{Re}\,p_n$ exceeds 10^{308}, the largest number that may be represented in double precision arithmetic.) We then perform this calculation for each pixel on a 628×628 grid representing the complex-θ_0 plane. We assign a colour to each pixel corresponding to the time at which p_n becomes infinite: White indicates that p_n does not become infinite within 400 time steps, and darker shades indicate that p_n becomes infinite after shorter times.

In figure 7 we display the results of this calculation for $K = 0.01$, 0.1, 0.2 and 0.6, and in figure 8 we display the results for this calculation for $K = 0.9$, 1.1, 2.0 and 5.0. Note that all these figures exhibit a complicated dendritic and fractal-like structure. A number of qualitative changes occur as K increases past its critical value. One obvious change is that the dendritic landscape becomes smoother and more rounded as K increases. A less obvious change is that the regions in which $\mathrm{Re}\,p_n$ does not diverge for $n \leq 400$ become connected when K exceeds K_c.

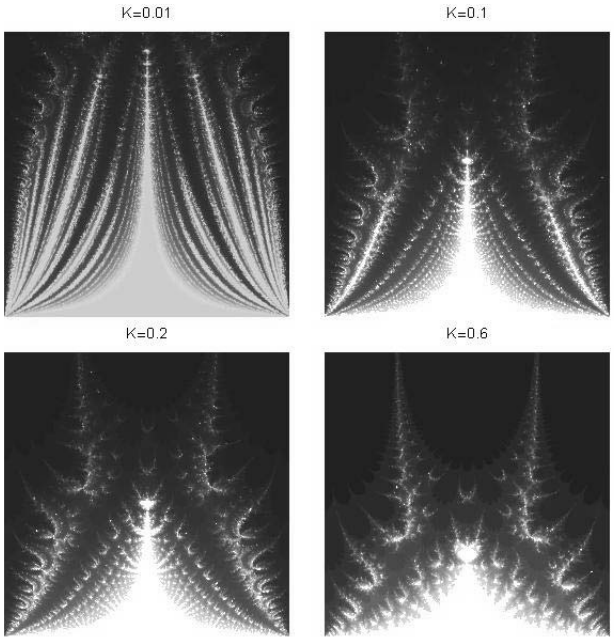

Figure 7. Behaviour of the solution to the kicked rotor in the complex-θ plane for four real values of K and a range of complex initial conditions: $p_0 = 0$, $0 \leq \mathrm{Re}\,\theta_0 \leq 2\pi$ and $0 \leq \mathrm{Im}\,\theta_0 \leq 2\pi$. We allow the system to evolve for at most $n = 400$ time steps. We assign a colour to each value of θ_0 according to the time at which $\mathrm{Re}\,p_n$ becomes infinite (if it does so). The graph of initial values of θ clearly has fractal structure. Distinctive changes occur in the nature of these complex plots as K increases.

Instead of constraining K to be real, we can, of course, take K to be complex. In figure 9 we take $K = 0.6i$. Note that the fractal structure in figures 7 and 8 is preserved, but it is distorted and loses its left–right symmetry.

Rather than requiring that K passes its critical value on the real-K axis, it is possible to go from a subcritical real value to a supercritical real value via a path in the complex-K plane, as in figure 10. The pictures making up this figure are constructed from values of K that lie on a semicircle of radius 0.6 and are centred at the critical value $K_{\mathrm{c}} = 0.9716\ldots$. In these figures we observe fractal structures like those in figures 7–9, but they are slightly distorted. However, there is a significant difference in that there is mottling (replacement of large patches of solid shading by a speckled pattern) in the graphs where K is complex; this mottling is absent when K is pure real or pure imaginary. (Note that when K is complex, $\mathcal{PT}$ symmetry is broken if the $\mathcal{T}$ operator is antilinear, that is, it changes the sign of i [33a].

We have performed a related study for the double pendulum: We allow g to be complex and repeat the numerical analysis of the short-time behaviour that we used to produce figure 3. We find that as the imaginary part of g increases, the fractal-like structure that we see in figure 3 gradually moves outward towards the corners of the figure. Correspondingly, the boundaries between different coloured

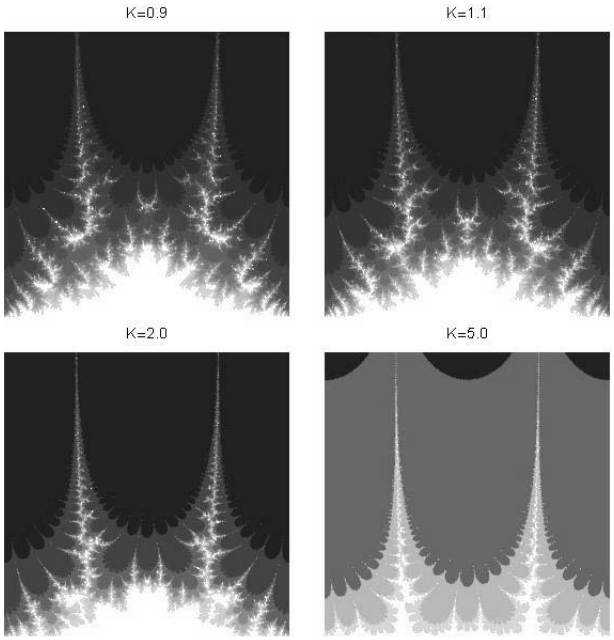

Figure 8. Same as in figure 7 with four higher values of K. There are many qualitative changes that occur as K increases. For example, the dendritic landscape that occurs for smaller values of K becomes smoother and more rounded as K increases. A subtle but important change is that the white regions, the regions in which $\mathrm{Re}\, p_n$ does not diverge for $n \leq 400$, become connected when K exceeds K_c.

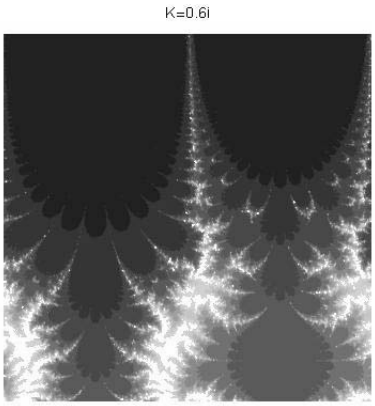

Figure 9. Same as in figures 7 and 8 except that $K = 0.6i$. Observe that while many features of the fractal structure in figures 7 and 8 are preserved, they are distorted and the left-right symmetry is destroyed.

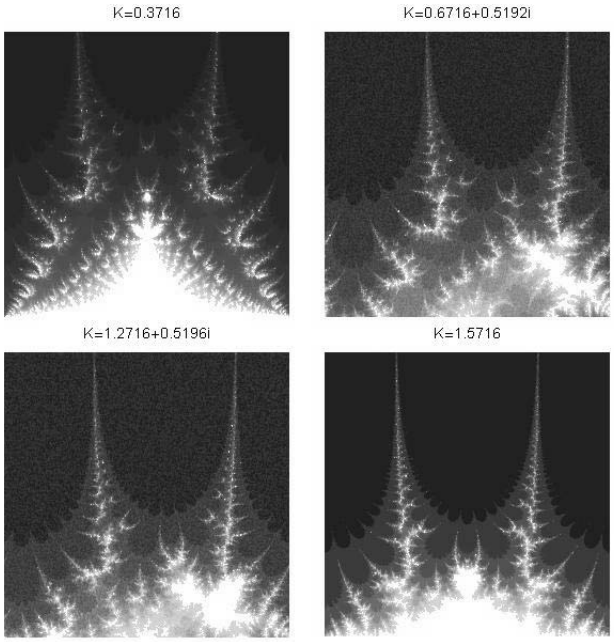

Figure 10. Same as in figure 7 except that the pictures making up this figure are constructed from values of K lying on a semicircle of radius 0.6 and centred at the critical value $K_c = 0.9716\ldots$. In these figures we observe fractal structures similar to those in figures 7–9, but slightly distorted. An important difference between this figure and figures 7–9 is that there is mottling (speckling) in those graphs where K is complex.

regions become smoother. To demonstrate this effect, we choose four different complex values, $g = 0.1 + 0.005i$, $0.1 + 0.01i$, $0.1 + 0.1i$, $0.1i$, and plot the results in figure 11.

5. Long-time behaviour

In this section we study the long-time behaviour of the kicked rotor and the double pendulum in complex phase space and we find that they share many qualitative features in this regime as well. By long-time we mean roughly 10^4 to 10^5 time steps or time units rather than the 10^3 time steps taken in §4. We find that the solutions to the dynamical equations for these systems exhibit characteristic behaviours at different time scales. On a long-time scale, which is determined by the imaginary part of the initial value of an angle, the solutions tend to ring; that is, the envelope of the solution grows and decays to zero with gradually changing periods. On a short-time scale the solution exhibits a distinct and clearly identifiable rapid oscillation, as we can see in figure 12.

We use the language of multiple-scale perturbation theory here [34] to describe this oscillatory behaviour. However, for both the kicked rotor and the double

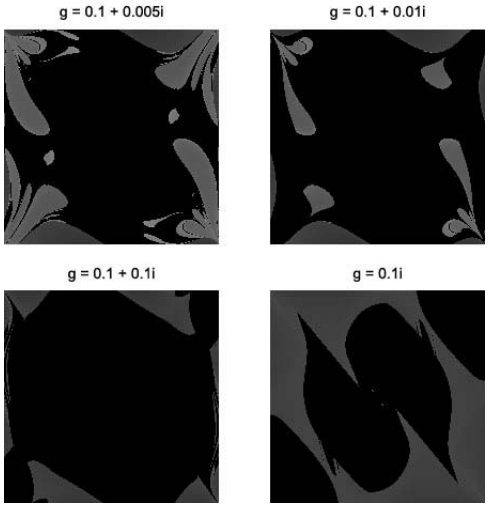

Figure 11. Short-time behaviour of the double pendulum with complex g. Same as figure 3 but with $g = 0.1 + 0.005i$, $0.1 + 0.01i$, $0.1 + 0.1i$, $0.1i$. As $\mathrm{Im}\, g$ increases, the fractal-like structure seen in figure 3 moves outward and towards the corners, and boundaries between differently coloured regions become smooth. Unlike figure 3, there are no energetically-forbidden-flip regions because there exist complex pathways from any pixel to a flipped configuration.

pendulum the unperturbed equations are not linear, and thus the usual techniques of multiple-scale perturbation theory cannot be applied directly in these cases.

Let us first examine the kicked rotor. As an initial condition we choose $p_0 = 0$ and $\theta_0 = 1 + i\epsilon$. In figure 12 we take $K = 0.6$ and $\epsilon = 10^{-5}$ and we plot $\mathrm{Re}\,\theta_n$, $\mathrm{Im}\,\theta_n$, $\mathrm{Re}\,p_n$ and $\mathrm{Im}\,p_n$ for $0 \leq n \lesssim 260\,000$. Note that while $\mathrm{Re}\,\theta_n$ and $\mathrm{Re}\,p_n$ oscillate within almost constant boundaries, $\mathrm{Im}\,\theta_n$ and $\mathrm{Im}\,p_n$ appear to ring with a period of order $1/\epsilon$. To verify this dependence on ϵ we take $\epsilon = 10^{-4}$, which is ten times larger, and we do not change the other initial conditions or the value of K. The result for $\mathrm{Im}\,\theta_n$ is given in figure 13, where we see that the period of the ringing is roughly ten times shorter than the period in figure 12. In both of these figures the ringing eventually comes to an abrupt end, at which point the iteration diverges and the amplitude of oscillation becomes infinite; this happens after about $2\frac{1}{2}$ rings in figure 12 and after about 11 rings in figure 13.

While the inverse of the imaginary part of θ_0 appears to set the scale of the ringing period, we have found that the length of the ringing period is also sensitive to the value of K. In figure 14 we plot $\mathrm{Im}\,p_n$ for four values of K: 0.5, 0.53, 0.55 and 1.0. For each of these values of K we plot $\mathrm{Im}\,p_n$ until it diverges. The initial conditions for each graph in figure 14 are the same as those in figure 12.

The double pendulum exhibits a long-time ringing behaviour that almost exactly parallels that of the kicked rotor. We plot the long-time behaviour of $\mathrm{Im}\,\theta_1$ for $g = 1$ and initial conditions $p_1(0) = p_2(0) = 0$, $\theta_1(0) = 1$ and $\theta_2(0) = 10^{-4}i$ in figure 15 and for $\theta_2(0) = 2 \times 10^{-4}i$ in figure 16. Note that, like the kicked rotor, the

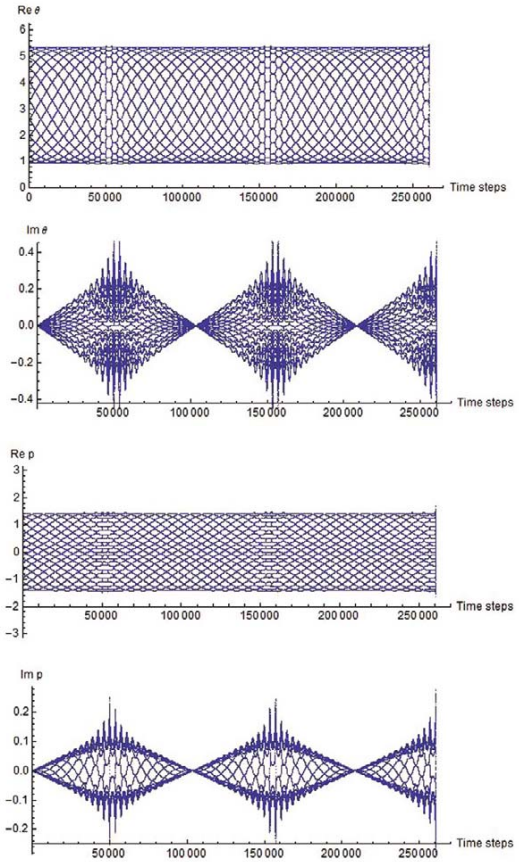

Figure 12. Long-time behaviour of the kicked rotor with initial conditions $p_0 = 0$ and $\theta_0 = 1 + 10^{-5}i$ and $K = 0.6$. While the real parts of p_n and θ_n oscillate between almost constant boundaries, the imaginary parts of p_n and θ_n exhibit a synchronized ringing behaviour whose period is of order $1/(\operatorname{Im}\theta_0)$. In addition to the long-time ringing there is a short-time oscillation that becomes most pronounced when the amplitude of the ringing is at a maximum. After about $2\frac{1}{2}$ rings the solution abruptly diverges and ceases to exist.

long-time scale ringing periods are determined by the imaginary part of the initial value of an angle; here, the period is proportional to $1/[\operatorname{Im}\theta_2(0)]$.

6. Concluding remarks

Apart from making the obvious remark that the two nonlinear systems studied in this paper exhibit very similar short-time and long-time dynamical behaviours, this work indicates that studying the dynamics of classical chaotic systems in complex phase space may help us to understand the onset of chaos. For example, for the

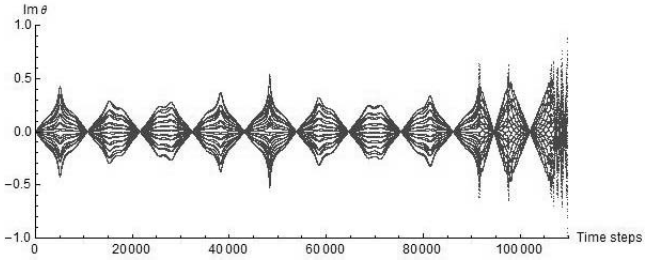

Figure 13. Same as in figure 12 except that the imaginary part of θ_0 is ten times smaller: $\theta_0 = 1 + 10^{-4}i$ and only the imaginary part of θ_n is displayed. In this figure the period of the ringing is ten times shorter and there are about 11 rings before the solution destabilizes and ceases to exist.

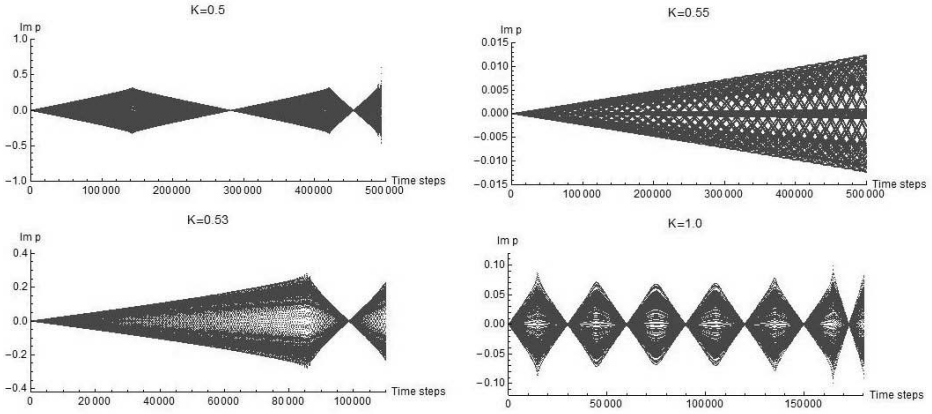

Figure 14. Long-time behaviour of $\mathrm{Im}\, p_n$ for the kicked rotor for four different values of K. The initial conditions are the same as in figure 12. Observe that the period of ringing is quite sensitive to the value of K.

case of the kicked rotor, we observe in figure 5 a change in the complex behaviour as K increases past K_c. Of course, the results reported here are empirical, but they clearly underscore the need for a deeper analytical understanding of these models. For example, an important unanswered question is, what is the analog of the KAM theorem in complex phase space?

Finally, we remark that the kicked rotor is one of the rare time-dependent systems whose quantum dynamics may be studied in detail. Indeed, the kicked rotor is a paradigm for studying quantum chaos. It might be useful to explore the $\mathcal{PT}$-deformed analog of the work of Fishman *et al* and Jain [19] because (i) this would be a nontrivial extension of $\mathcal{PT}$ quantum mechanics to time-dependent systems and (ii) it may help to define and understand $\mathcal{PT}$-symmetric quantum chaos.

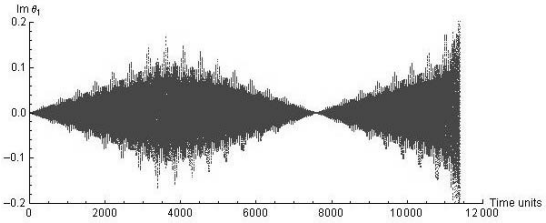

Figure 15. Long-time behaviour of the double pendulum with $g = 1$. The initial conditions used for this plot are $p_1(0) = p_2(0) = 0$, $\theta_1(0) = 1$ and $\theta_2(0) = 10^{-4}i$. Like the kicked rotor, the imaginary part of an angle exhibits a ringing behaviour whose characteristic period is of order $1/\mathrm{Im}\,\theta_2(0)$. The plot terminates when the solution to the equations of motion abruptly diverges. Like the kicked rotor, there is also a short-time oscillation, but unlike the kicked rotor, the positive and negative peaks are out of phase with one another.

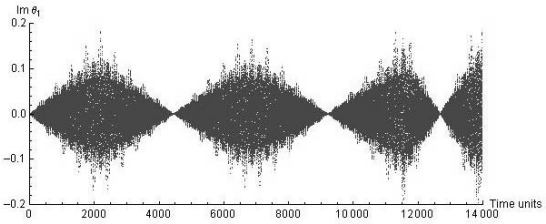

Figure 16. Same as figure 15 but with $\theta_2(0) = 2\times10^{-4}i$. Note that doubling the imaginary part of $\theta_2(0)$ has the effect of roughly halving the ringing period.

Acknowledgements

We thank S Fishman and F Leyvraz for discussions and I Guarnery for bringing ref. [27] to our attention. CMB is supported by the U.S. Department of Energy. JF thanks the KITP at UC Santa Barbara for its hospitality while this paper was completed. His research at the KITP was supported in part by the National Science Foundation under Grant No. PHY05-51164. DWH is supported by Symplectic Ltd. DJW thanks the Imperial College High Performance Computing Service, URL: http: // www.imperial.ac.uk / ict/services / teachingandresearchservices/highperformancecomputing.

References

[1] C M Bender, *Contemp. Phys.* **46**, 277 (2005); *Rep. Prog. Phys.* **70**, 947 (2007)
[2] P Dorey, C Dunning and R Tateo, *J. Phys. A: Math. Gen.* **40**, R205 (2007)
[3] C M Bender, S Boettcher and P N Meisinger, *J. Math. Phys.* **40**, 2201 (1999)

[4] A Nanayakkara, *Czech. J. Phys.* **54**, 101 (2004); *J. Phys. A: Math. Gen.* **37**, 4321 (2004)
[5] C M Bender, J-H Chen, D W Darg and K A Milton, *J. Phys. A: Math. Gen.* **39**, 4219 (2006)
[6] C M Bender and D W Darg, *J. Math. Phys.* **48**, 042703 (2007)
[7] C M Bender, D D Holm and D W Hook, *J. Phys. A: Math. Theor.* **40**, F81 (2007)
[8] C M Bender, D D Holm and D W Hook, *J. Phys. A: Math. Theor.* **40**, F793 (2007)
[9] C M Bender, D C Brody, J-H Chen and E Furlan, *J. Phys. A: Math. Theor.* **40**, F153 (2007)
[10] A Fring, *J. Phys. A: Math. Theor.* **40**, 4215 (2007)
[11] C M Bender and J Feinberg, *J. Phys. A: Math. Theor.* **41**, 244004 (2008)
[12] C M Bender and D W Hook, *J. Phys. A: Math. Theor.* **41**, 244005 (2008)
[13] C M Bender, D C Brody and D W Hook, *J. Phys. A: Math. Theor.* **41**, 352003 (2008)
T Arpornthip and C M Bender, *Pramana – J. Phys.* **73**, 259 (2009)
[14] A V Smilga, *J. Phys. A: Math. Theor.* **41**, 244026 (2008)
[15] A V Smilga, *J. Phys. A: Math. Theor.* **42**, 095301 (2009)
[16] S Ghosh and S K Modak, *Phys. Lett.* **A373**, 1212 (2009)
[17] E Ott, *Chaos in dynamical systems* (Cambridge University Press, Cambridge, 2002), 2nd ed.
[18] M Tabor, *Chaos and integrability in nonlinear dynamics: An introduction* (Wiley-Interscience, New York, 1989)
[19] S Fishman, Quantum Localization in Quantum Chaos, *Proc. of the International School of Physics "Enrico Fermi"*, Varenna, July 1991 (North-Holland, New York, 1993)
S R Jain, *Phys. Rev. Lett.* **70**, 3553 (1993)
S Fishman, Quantum Localization in Quantum Dynamics of Simple Systems, *Proc. of the 44th Scottish Universities Summer School in Physics*, Stirling, August 1994, edited by G L Oppo, S M Barnett, E Riis and M Wilkinson (SUSSP Publications and Institute of Physics, Bristol, 1996)
S Fishman, D R Grempel and R E Prange, *Phys. Rev. Lett.* **49**, 509 (1982)
D R Grempel, R E Prange and S Fishman, *Phys. Rev.* **A29**, 1639 (1984)
[20] P H Richter and H-J Scholz, *Chaos in classical mechanics: The double pendulum* in *stochastic phenomena and chaotic behaviour in complex systems* edited by P Schuster (Springer-Verlag, Berlin, 1984)
[21] J S Heyl, http://tabitha.phas.ubc.ca/wiki/index.php/Double_pendulum (2007)
[22] A J Lichtenberg and M A Lieberman, *Regular and stochastic motion* (Springer-Verlag, New York, 1983)
[23] D Ben-Simon and L P Kadanoff, *Physica* **D13**, 82 (1984)
R S MacKay, J D Meiss and I C Percival, *Phys. Rev. Lett.* **52**, 697 (1984); *Physica* **D13**, 55 (1984)
I Dana and S Fishman, *Physica* **D17**, 63 (1985)
[24] B V Chirikov, *Phys. Rep.* **52**, 263 (1979)
[25] D L Shepelyansky, *Physica* **D8**, 208 (1983)
[26] J M Greene, *J. Math. Phys.* **20**, 1183 (1981)
[26a] The idea to study chaotic systems in complex phase space was introduced in ref. [27]. The motivation in these papers was to study the effects of classical chaos on semiclassical tunnelling. In the instanton calculus one must deal with a complex configuration space. Additional complex studies are found in refs [28–30]
[27] A Ishikawa, A Tanaka and A Shudo, *J. Phys. A: Math. Theor.* **40**, F397 (2007)
T Onishi, A Shudo, K S Ikeda and K Takahashi, *Phys. Rev.* **E68**, 056211 (2003)

A Shudo, Y Ishii and K S Ikeda, *J. Phys. A: Math. Gen.* **35**, L31 (2002)
T Onishi, A Shudo, K S Ikeda and K Takahashi, *Phys. Rev.* **E64**, 025201 (2001)
[28] J M Greene and I C Percival, *Physica* **D3**, 540 (1982)
I C Percival, *Physica* **D6**, 67 (1982)
[29] A Berretti and L Chierchaia, *Nonlinearity* **3**, 39 (1990)
A Berretti and S Marmi, *Phys. Rev. Lett.* **68**, 1443 (1992)
S Marmi, *J. Phys.* **A23**, 3447 (1990)
[30] V F Lazutkin and C Simo, *Int. J. Bifurcation Chaos Appl. Sci. Eng.* **2**, 253 (1997)
[31] R I McLachlan and P Atela, *Nonlinearity* **5**, 541 (1992)
[32] B Leimkuhler and S Reich, *Simulating Hamiltonian dynamics* (Cambridge University Press, Cambridge, 2004)
[33] These qualitative changes in behaviour were mentioned briefly in talks given by C M Bender and D W Hook at the *Workshop on Pseudo-Hermitian Hamiltonians in Quantum Physics VI*, held in London, July 2007.
[33a] When K and g become imaginary the system becomes invariant under combined $\mathcal{PT}$ reflection. However, now $\mathcal{P}$ is the spatial reflection, $\mathcal{P}$: $\theta \to \theta + \pi$, so that both $\cos\theta$ and $\sin\theta$, and thus the Cartesian coordinates, change sign. The sign of the angular momentum now remains unchanged under parity reflection. This explains the symmetry of the plots when K and g are pure imaginary (see figure 9 and the lower-right plot in figure 11 respectively). This change of symmetry of the system as its couplings vary in complex parameter space is not unusual. For example, at a generic point in coupling space for the three-dimensional anisotropic harmonic oscillator, the only symmetry is parity. However, when any two couplings coincide and are different from the third, the reflection symmetry is enhanced and becomes a continuous symmetry, namely, an $O(2)$ symmetry around the third axis. (There remains parity-time reflection symmetry in the third direction.) When all three couplings coincide, the symmetry is enhanced further and becomes a full $O(3)$ symmetry
[34] C M Bender and S A Orszag, *Advanced mathematical methods for scientists and engineers* (McGraw Hill, New York, 1978)